

# Mesoscopic model for the fluctuating hydrodynamics of binary and ternary mixtures

E. TÜZEL, G. PAN, T. IHLE and D.M. KROLL

*Department of Physics, North Dakota State University, P.O. Box 5566, Fargo, ND 58105, USA*

PACS 02.70.Ns – Molecular dynamics and particle methods

PACS 47.11.-j – Computational methods in fluid dynamics

PACS 05.40.-a – Fluctuation phenomena, random processes, noise, and Brownian motion

**Abstract.** - A recently introduced particle-based model for fluid dynamics with continuous velocities is generalized to model immiscible binary mixtures. Excluded volume interactions between the two components are modeled by stochastic multiparticle collisions which depend on the local velocities and densities. Momentum and energy are conserved locally, and entropically driven phase separation occurs for high collision rates. An explicit expression for the equation of state is derived, and the concentration dependence of the bulk free energy is shown to be the same as that of the Widom-Rowlinson model. Analytic results for the phase diagram are in excellent agreement with simulation data. Results for the line tension obtained from the analysis of the capillary wave spectrum of a droplet agree with measurements based on the Laplace's equation. The introduction of “amphiphilic” dimers makes it possible to model the phase behavior and dynamics of ternary surfactant mixtures.

**Introduction.** – Hydrodynamic interactions and thermal fluctuations play a crucial role in a wide range of phenomena in soft matter physics and molecular and cellular biology. Because of the complexity of these systems, simulations have played an essential role in much of the research in these areas. In fact, the wide range of length and time scales in these problems places severe requirements on simulation protocol, and has lead to the development of several new coarse-grained, mesoscale simulation techniques such as lattice gas automata [1], the lattice Boltzmann method [2], dissipative particle dynamics [3,4], smoothed particle hydrodynamics [5], and a newer approach variously called multi-particle collision dynamics or stochastic rotation dynamics (SRD) [6]. The basic motivation of all these approaches is to coarse-grain out irrelevant atomistic details while correctly incorporating the essential physics and conservation laws.

SRD has several attractive features which have lead to its use in studies ranging from sedimentation in colloidal suspensions [7] to the dynamic behavior of polymers in solution [8,9] and vesicles in flow [10]. In particular, it enables simulations in the microcanonical ensemble while fully incorporating both hydrodynamic interactions and thermal fluctuations; in addition, because SRD is a particle-based method, the coupling to colloidal particles, polymers, or other aggregates is straightforward, and the Brownian motion of these embedded objects is realized in a very natural way—through random collisions with the solvent particles. Finally, the simplicity of the algorithm has made it possible to obtain accurate analytic expressions for the transport coefficients [11–13].

Recently, it has been shown how to generalize the multi-particle collisions of the original SRD algorithm to model excluded volume effects, allowing for a more realistic modeling of dense gases and liquids with a nonideal equation of state [14, 15]. In this Letter we show that a similar approach can be used to model immiscible binary mixtures. The resulting model retains much of the simplicity of the original SRD algorithm, allowing for a detailed analysis of the transport coefficients and an explicit calculation of the equation of state and the bulk entropy and free energy densities. Since there is no potential energy, all interactions in the model are entropic, and the resulting bulk free energy density is the same as that of the Widom-Rowlinson model [16]. Theoretical predictions for the phase diagram are shown to be in good agreement with simulation data, and results for the line tension obtained from an analysis of the spectrum of capillary wave fluctuations agree with measurements based on the Laplace equation.

**Model.** — In a binary mixture of A and B particles, phase separation can occur when there is an effective repulsion between A-B pairs. In the current model, this is achieved by introducing multi-particle collisions between A and B particles. The fluid is modeled by a large number  $N$  of point-like particles of unit mass which move in continuous space with a continuous distribution of velocities. There are  $N_A$  and  $N_B$  particles of type A and B, respectively. In two dimensions, the system is coarse-grained into  $(L/a)^2$  cells of a square lattice of linear dimension  $L$  and lattice constant  $a$ . The generalization to three dimensions is straightforward.

To define the collisions, we introduce a second grid with sides of length  $2a$  which groups four adjacent cells into one “supercell”. As discussed in [17], Galilean invariance requires that the collisions occur in a randomly shifted grid. All particles are shifted by the *same* random vector with components in the interval  $[-a, a]$  before the collision step. Particles are then shifted back by the same amount after the collision. To initiate a collision, pairs of cells in every supercell are selected at random. As shown in Fig. 1, three different choices are possible: a) horizontal (with  $\sigma_1 = \hat{x}$ ), b) vertical ( $\sigma_2 = \hat{y}$ ), and c) diagonal collisions (with  $\sigma_3 = (\hat{x} + \hat{y})/\sqrt{2}$  and  $\sigma_4 = (\hat{x} - \hat{y})/\sqrt{2}$ ). For each pair of cells, two types of collisions are possible. As illustrated in Fig. 1, particles of type A in the first cell can undergo a collision with particles of type B in the second cell; vice versa, particles of type B in the first cell can undergo a collision with particles of type A in the second cell. There are no A-A or B-B collisions, so that there is an effective repulsion between A-B pairs. The rules and probabilities for these collisions are chosen in the same way as in the nonideal single-component fluid described in Refs. [14, 18]. For example, consider the collision of A particles in the first cell with the B particles in the second. The mean particle velocity of A particles in the first cell is  $\mathbf{u}_A = (1/m_A) \sum_{i=1}^{m_A} \mathbf{v}_i$ , where the sum runs over all A particles,  $m_A$ , in the first cell. Similarly,  $\mathbf{u}_B = (1/m_B) \sum_{i=1}^{m_B} \mathbf{v}_i$  is the mean velocity of B particles in the second cell. The projection of the difference of the mean velocities of the selected cell-pairs on  $\sigma_j$ ,  $\Delta u_{AB} = \sigma_j \cdot (\mathbf{u}_A - \mathbf{u}_B)$ , is then used to determine the probability of collision. If  $\Delta u_{AB} < 0$ , no collision will be performed. For positive  $\Delta u_{AB}$ , a collision will occur with an acceptance probability

$$p_A(m_A, m_B, \Delta u_{AB}) = \max\{1, A m_A m_B \Delta u_{AB} \Theta(\Delta u_{AB})\}, \quad (1)$$

where  $\Theta$  is the unit step function and  $A$  is a parameter which allows us to tune the equation of state; in order to ensure thermodynamic consistency, it must be sufficiently small that  $A m_A m_B \Delta u_{AB} \Theta(\Delta u_{AB}) < 1$  for essentially all collisions [15]. When a collision occurs, the parallel component of the mean velocities of colliding particles in the two cells is exchanged,  $v_i^\parallel(t + \tau) - u_{AB}^\parallel = -(v_i^\parallel(t) - u_{AB}^\parallel)$ , where  $u_{AB}^\parallel = (m_A u_A^\parallel + m_B u_B^\parallel)/(m_A + m_B)$  is the parallel component of the mean velocity of the colliding particles. The perpendicular component remains unchanged. It is easy to verify that these rules conserve momentum and energy in the cell pairs. The collision of B particles in the first cell with A particles in the second is handled in a similar fashion.

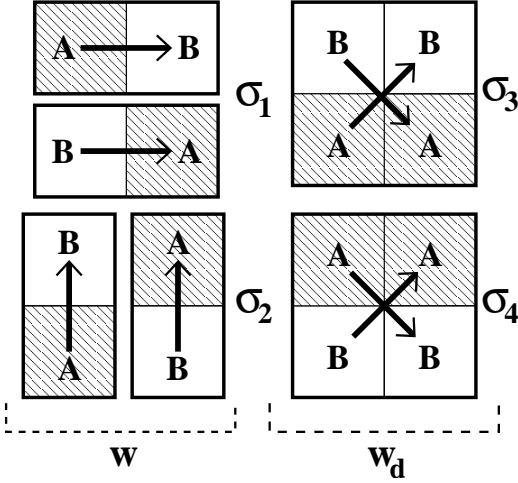


Fig. 1

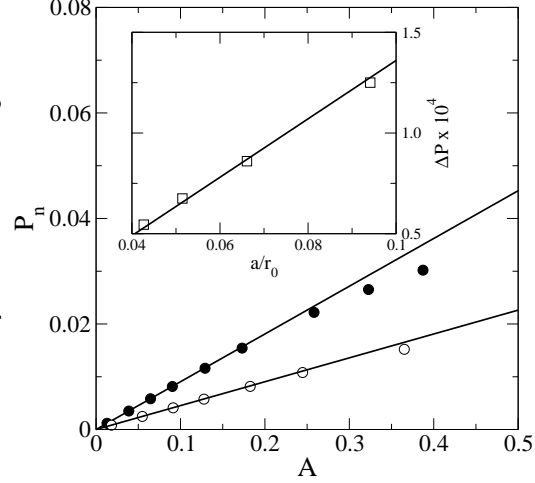


Fig. 2

Fig. 1: Schematic binary collision rules. Momentum is exchanged in three ways: a) horizontally along  $\sigma_1$ , b) vertically along  $\sigma_2$ , and c) diagonally along  $\sigma_3$  and  $\sigma_4$ .  $w$  and  $w_d$  denote the probabilities of choosing collisions a), b) and c), respectively. For a cell pair defined by the vector  $\sigma$ , A particles in one cell collide with B particles in the other cell, and vice versa.

Fig. 2: Non-ideal contribution to the pressure,  $P_n$ , (in units of  $k_B T/a^2$ ) as a function of the tuning parameter  $A$  (in units of  $\tau/a$ ). The bullets ( $\bullet$ ) and open circles ( $\circ$ ) are results for  $k_B T = 0.006$  and  $k_B T = 0.003$ , respectively. The lines are plots of Eq. (7). The inset shows the pressure difference across a droplet interface as a function of the inverse droplet radius, for  $A = 0.60$  at  $k_B T = 0.0005$ . The pressure is measured using the expression given in Eq. (8). The solid line is a plot of Eq. (13), using the line tension obtained from the analysis of capillary waves. Parameters:  $L/a = 64$ ,  $M_A \equiv N_A/(L/a)^2 = 5$ ,  $M_B \equiv N_B/(L/a)^2 = 5$ ,  $a = 1$ , and  $\tau = 1.0$ .

Because there are no A-A and B-B collisions, additional SRD collisions at the cell level are incorporated in order to mix particle momenta. The order of A-B and SRD collision is random, i.e., the SRD collision is performed first with a probability of one half. If necessary, the viscosity can be tuned by not performing SRD collisions every time step. The results presented in this Letter were obtained using a SRD collision angle of  $90^\circ$ .

**Transport Coefficients.** – The transport coefficients can be determined using the same Green-Kubo formalism as for the original SRD algorithm [11,17,19] and its extensions [14,15,18]. In particular, the discrete Green-Kubo relation

$$\Lambda_{\alpha\beta}(\hat{\mathbf{k}}) = \frac{\tau}{Nk_B T} \sum_{n=0}^{\infty} g_{\alpha\beta}(\hat{\mathbf{k}}; n\tau), \quad (2)$$

with  $g_{\alpha\beta}(\hat{\mathbf{k}}; t) \equiv \langle \hat{k}_\lambda \sigma_{\alpha\lambda}(0) | \hat{k}_{\lambda'} \sigma_{\beta\lambda'}(t) \rangle$ , expresses the matrix of viscous transport coefficients,  $\Lambda_{\alpha\beta}(\hat{\mathbf{k}})$ , in terms of a sum of time correlation functions of the reduced fluxes

$$\hat{k}_\lambda \sigma_{\alpha\lambda}(t) \equiv \frac{1}{\tau} \sum_{j=1}^N \left( v_{j\alpha}(t) \hat{\mathbf{k}} \cdot \Delta \boldsymbol{\xi}_j(t) + \Delta v_{j\alpha}(t) \hat{\mathbf{k}} \cdot [\Delta \boldsymbol{\xi}_j^s(t) - \mathbf{z}_{jl}^s(t+\tau)/2] - \frac{\tau \hat{k}_\alpha}{d} v_j^2(t) \right), \quad (3)$$

where  $\Delta \boldsymbol{\xi}_j(t) = \boldsymbol{\xi}_j(t+\tau) - \boldsymbol{\xi}_j(t)$ ,  $\Delta v_{j\alpha}(t) = v_{j\alpha}(t+\tau) - v_{j\alpha}(t)$  and  $\Delta \boldsymbol{\xi}_j^s(t) = \boldsymbol{\xi}_j^s(t+\tau) - \boldsymbol{\xi}_j^s(t+\tau)$ .  $\tau$  is the time step in the simulation and the prime on the sum in Eq. (2) indicates that the  $n = 0$  term has the relative weight  $1/2$ .  $\boldsymbol{\xi}_j(t)$  is the cell coordinate of particle  $j$  at time  $t = n\tau$ , while  $\boldsymbol{\xi}_j^s$  is its cell coordinate in the (stochastically) shifted frame.  $\mathbf{z}_{jl}^s(\tau)$

indexes pairs of cells which participate in a collision event at time  $\tau$ ; the second subscript,  $l$ , is the index of the collision vectors  $\boldsymbol{\sigma}_l$  shown in Fig. 1. For example, for collisions characterized by  $\boldsymbol{\sigma}_1$ ,  $z_{j1x}^s = 1$  if  $\xi_{jx}^s$  in Eq. (3) is one of the two cells on the left of a supercell and  $z_{j1x}^s = -1$  if  $\xi_{jx}^s$  is on the right hand side of a supercell; all other components of  $\mathbf{z}_{j1}^s$  are zero. In general [18], the components of  $\mathbf{z}_{jl}^s$  are either 0, 1, or  $-1$ .

Assuming only cubic symmetry, the most general form of  $\Lambda_{\alpha\beta}(\hat{\mathbf{k}})$  in two dimensions is [11]

$$\Lambda_{\alpha\beta}(\hat{\mathbf{k}}) \equiv \nu_1 \delta_{\alpha\beta} + \nu_2 \left( \delta_{\alpha\beta} - \hat{k}_\alpha \hat{k}_\beta \right) + \gamma \hat{k}_\alpha \hat{k}_\beta + \epsilon \hat{k}_\gamma \hat{k}_\rho I_{\alpha\beta\gamma\rho}, \quad (4)$$

where  $\overleftrightarrow{I}$  is the rank four unit tensor.  $\nu_2$  is a new viscous transport coefficient associated with the non-symmetric part of the stress tensor,  $\gamma$  is the bulk viscosity and  $\epsilon$  is a viscosity coefficient which is nonzero only if there is cubic anisotropy. In a simple liquid,  $\epsilon = 0$  (because of invariance with respect to infinitesimal rotations),  $\nu = \nu_1$ , and  $\nu_2 = 0$  (because the stress tensor is symmetric in  $\partial_\alpha v_\beta$ ).

Since both particle streaming and the collisions contribute to momentum transport, there are two—kinetic and collisional—contributions to the transport coefficients. The kinetic contribution dominates at large mean free paths,  $\lambda$ , the collisional for  $\lambda/a \ll 1$ . For the original SRD algorithm, the kinetic contribution is isotropic, so that there is only one viscosity,  $\nu$ ; the kinetic contribution to the bulk viscosity is also zero, as in a real ideal gas [13]. However, because SRD collisions do not, in general, conserve angular momentum, the microscopic stress tensor is not symmetric and there is a collisional contribution [11] to  $\nu_2$ . It should be noted, however, that the SRD algorithm can be modified to conserve angular momentum in two dimensions by introducing a unique, configuration dependent collision angle in each cell [20].

In Refs. [14,18] it was argued (for the nonideal model) that the probabilities of horizontal and vertical ( $w$ ) and diagonal ( $w_d$ ) collisions should be chosen so that the relaxation rate of the second moments of the velocity distribution function all decay at the same rate. This lead to the requirement that  $w = 1/4$  and  $w_d = 1/2$ . Here we show that the same result follows from the requirement that the kinetic contribution to the viscous stress tensor is symmetric, so that there is only one viscosity, and  $\epsilon = \gamma - \nu_2 = 0$ . To see this, note first that for  $\alpha = \beta = 1$  with  $\hat{\mathbf{k}} = \hat{y}$  and  $\hat{\mathbf{k}} = \hat{x}$ , Eqs. (2)-(4) give  $\gamma - \nu_2 = -\epsilon/2 = [\Lambda_{11}(\hat{y}) - \Lambda_{11}(\hat{x})]$  and  $\nu_1 + \nu_2 = \Lambda_{11}(\hat{y})$ . For large mean free paths, the term in parentheses in Eq. (3) reduces to  $v_{j\alpha}(t) \hat{\mathbf{k}} \cdot \mathbf{v}_j(t) - (\tau \hat{k}_\alpha / 2) v_j^2(t)$  in two dimensions; using this result and making the assumption of molecular chaos, the sum in Eq. (2) reduces to a geometric series in  $g_{11}(\hat{\mathbf{k}}; \tau)$ . The calculation of these quantities requires that the contributions from the horizontal,  $g_{11}^H$ , vertical,  $g_{11}^V$ , and diagonal collisions,  $g_{11}^D$ , be calculated individually and then summed in the form

$$g_{11}(\hat{\mathbf{k}}; \tau) = w[g_{11}^H(\hat{\mathbf{k}}; \tau) + g_{11}^V(\hat{\mathbf{k}}; \tau)] + w_d g_{11}^D(\hat{\mathbf{k}}; \tau) . \quad (5)$$

If  $g_{11}(\hat{y}; \tau) \neq g_{11}(\hat{x}; \tau)$ , there is a cubic anisotropy. Ignoring fluctuations in the number of particles per cell, we find that  $g_{11}(\hat{y}; \tau) = g_{11}(\hat{x}; \tau)$  only if  $w = 1/4$  and  $w_d = 1/2$ . In this case, the only non-zero viscosity is

$$\nu \equiv \Lambda_{11}(\hat{y}) = \frac{\tau k_B T}{2} \left( \frac{1}{A} \sqrt{\frac{2\pi}{k_B T}} [M_A M_B (M_A + M_B)]^{-1/2} - 1 \right) , \quad (6)$$

where  $M_A \equiv N_A / (L/a)^2$  and  $M_B \equiv N_B / (L/a)^2$ . In deep quenches, the density of the minority phase is very small, and the nonideal contribution to the viscosity approaches zero, i.e.  $g(\tau) \sim 1 - O(\rho_A)$ ; in this case, the SRD collisions provide the dominant contribution to the viscosity.

**Free Energy.** — An analytic expression for the equation of state of this model can be derived by calculating the momentum transfer across a fixed surface, in much the same way

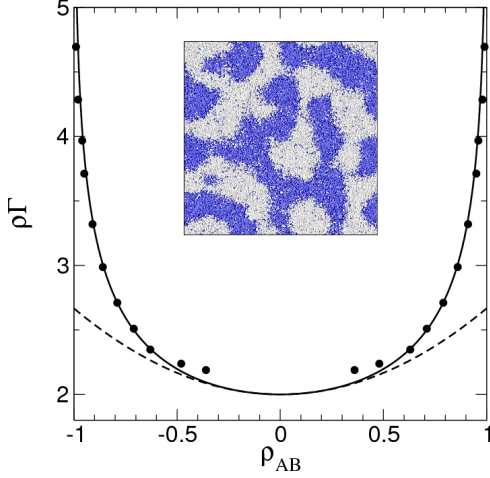


Fig. 3

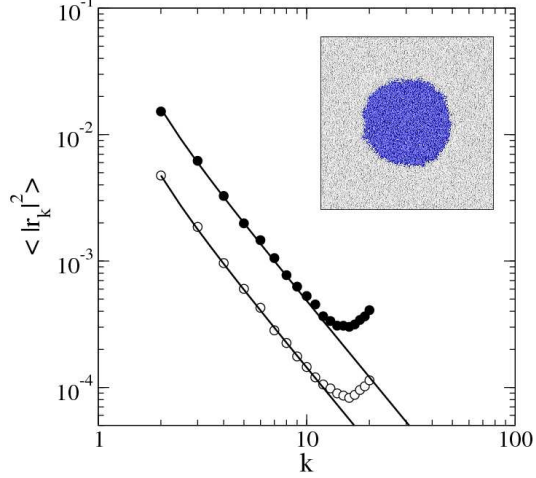


Fig. 4

Fig. 3: Phase diagram of a 50% A - 50% B mixture. There is phase separation for  $\rho\Gamma > 2$ . The inset shows a configuration 50,000 time steps after a quench along  $\rho_{AB} = 0$  to  $\rho\Gamma = 3.62$ . The dark (blue) and light (white) colored spheres are A and B particles, respectively. Parameters:  $L/a = 64$ ,  $M_A = M_B = 5$ ,  $k_B T = 0.0004$ ,  $\tau = 1$  and  $a = 1$ .

Fig. 4: Dimensionless radial fluctuations,  $\langle |r_k|^2 \rangle$ , as a function of the mode number  $k$  for  $A = 0.45$  (●) and  $A = 0.60$  (○), with  $k_B T = 0.0004$ . The average droplet radii are  $r_0 = 11.95 a$  and  $r_0 = 15.21 a$ , respectively. The solid lines are fits to Eq. (12). The inset shows a typical droplet configuration for  $A = 0.60$  and  $T = 0.0004$ . Parameters:  $L/a = 64$ ,  $M_A = 2$ ,  $M_B = 8$ ,  $a = 1$  and  $\tau = 1$ .

as was done for the nonideal model in Ref. [14]. The resulting expression for the nonideal contribution to pressure is

$$P_n = \left( w + \frac{w_d}{\sqrt{2}} \right) A M_A M_B \frac{k_B T}{a \tau} = \Gamma k_B T \rho_A \rho_B, \quad (7)$$

where  $\rho_A$  and  $\rho_B$  are the densities of A and B and  $\Gamma \equiv (w + w_d/\sqrt{2})a^3 A/\tau$ . In simulations, the total pressure can be measured by taking the ensemble average of the diagonal components of the microscopic stress tensor. In this way, the pressure can be measured locally, at the cell level. In particular, the pressure in a region consisting of  $N_c$  cells is

$$P = \frac{1}{\tau a^2 N_c} \left\langle \sum_{c=1}^{N_c} \sum_{i \in c} [\tau v_{jx}^2 - \Delta v_{jx} z_{jlx}^s / 2] \right\rangle, \quad (8)$$

where the second sum runs over the particles in cell  $c$ . The first term in Eq. (8) is the ideal gas contribution to the pressure; the second term comes from the momentum transfer between cells involved in the collision indexed by  $\mathbf{z}^s$ . The results of measurements of the non-ideal contribution to the pressure obtained using Eq. (8) are shown in Fig. 2 for  $k_B T = 0.006$  (●) and  $k_B T = 0.003$  (○). The lines are the theoretical predictions of Eq. (7). For small values of  $A$ , the agreement between theory and simulation is excellent; deviations for larger  $A$  are an indication that the model is no longer thermodynamically consistent [15].

Equation (7) can be used to determine the entropy density,  $s$ . The ideal gas contribution to  $s$  has the form [21]

$$s_{ideal} = \rho \varphi(T) - k_B [\rho_A \ln \rho_A + \rho_B \ln \rho_B], \quad (9)$$

where  $\rho = \rho_A + \rho_B$ . Since  $\varphi(T)$  is independent of  $\rho_A$  and  $\rho_B$ , this term does not play a role in the current discussion. The nonideal contribution to the entropy density,  $s_n$ , can be

obtained from Eq. (7) using the thermodynamic relation [21]

$$P_n/T = s_n - \rho_A \partial s_n / \partial \rho_A - \rho_B \partial s_n / \partial \rho_B. \quad (10)$$

The result is  $s_n = -k_B \Gamma \rho_A \rho_B$ , so that the total configurational contribution to the entropy density is

$$s = -k_B [\rho_A \ln \rho_A + \rho_B \ln \rho_B + \Gamma \rho_A \rho_B]. \quad (11)$$

Since there is no configurational contribution to the internal energy in this model, the mean field phase diagram can be determined by maximizing the entropy at fixed density  $\rho$ . The resulting demixing phase diagram as a function of  $\rho_{AB} \equiv (\rho_A - \rho_B)/\rho$  is given by the solid line in Fig. 3. The critical point is located at  $\rho_{AB} = 0$ ,  $(\rho\Gamma)^* = 2$ . For  $\rho\Gamma < 2$ , the order parameter  $\rho_{AB} = 0$ ; for  $\rho\Gamma > 2$ , there is phase separation into coexisting A and B-rich phases. Simulation results for  $\rho_{AB}$  obtained from density histograms are shown as bullets ( $\bullet$ ). The dashed line is a plot of the leading singular behavior,  $\rho_{AB} = \sqrt{3(\rho\Gamma - 2)/2}$ , of the order parameter at the critical point. As can be seen, the agreement between the mean field predictions and simulation are very good except close to the critical point, where the histogram method of determining the coexisting densities is unreliable and critical fluctuations could influence the shape of the coexistence curve.

**Line Tension.** — A configuration after 50,000 time steps following a quench to point  $\rho_{AB} = 0$ ,  $\rho\Gamma = 3.62$  of the phase diagram is shown in the inset to Fig. 3, and a snapshot of a fluctuating droplet at  $\rho_{AB} = -0.6$ ,  $\rho\Gamma = 3.62$  is shown in the inset to Fig. 4. The amplitude of the capillary wave fluctuations of a droplet is determined by the line tension,  $\sigma$ . In particular, for a droplet in an incompressible fluid, the mean square amplitude of fluctuations of the Fourier components of the (dimensionless) droplet radius,  $\langle |r_k|^2 \rangle$ , is related to the line tension by the dispersion relation [22]

$$\langle |r_k|^2 \rangle = \frac{2k_B T}{\pi r_0 \sigma} \left( \frac{1}{k^2 - 1} \right), \quad (12)$$

where  $r_0$  is the mean radius of the droplet. Fig. 4 contains a plot of  $\langle |r_k|^2 \rangle$  as a function of mode number  $k$  for  $A = 0.45$  ( $\rho\Gamma = 3.62$ ) and  $A = 0.60$  ( $\rho\Gamma = 2.72$ ). Fits to the data yield  $\sigma a/k_B T \simeq 2.9$  for  $\rho\Gamma = 3.62$  and  $\sigma a/k_B T \simeq 1.1$  for  $\rho\Gamma = 2.72$ . Mechanical equilibrium requires that the pressure difference across the interface of a droplet satisfies the Laplace equation,

$$\Delta p = p_{in} - p_{out} = \sigma/r_0. \quad (13)$$

Using Eq. (8), we have determined  $\Delta p$  as a function of the droplet radius for  $A = 0.60$  and  $k_B T = 0.0005$ . The results are plotted in the inset to Fig. 2, where it can be seen that the Laplace relation is satisfied for the correct values of the line tension.

The model therefore displays the correct thermodynamic behavior and interfacial fluctuations. It can also be extended to model amphiphilic mixtures by introducing dimers consisting of tethered A and B particles [22]. If the A and B components of the dimers participate in the same collisions as the solvent, they behave like amphiphilic molecules in oil-water mixtures. The resulting model displays a rich phase behavior as a function of  $\rho\Gamma$  and the number of dimers,  $N_d$ . We have observed both droplets and micelles, as shown in Fig. 5, and a bicontinuous phase, as illustrated in Fig. 6. The coarse-grained nature of the algorithm enables the study of large time scales with a feasible computational effort.

\* \* \*

Support from the National Science Foundation under Grant No. DMR-0513393 and ND EPSCoR through NSF grant EPS-0132289 are gratefully acknowledged.



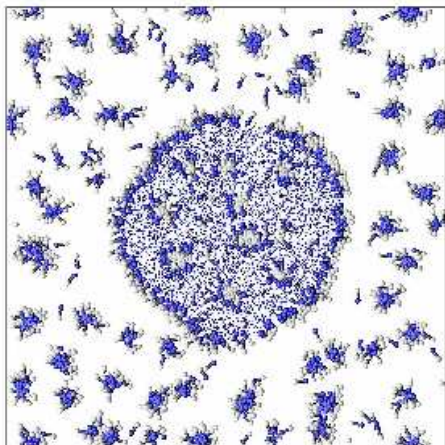


Fig. 5

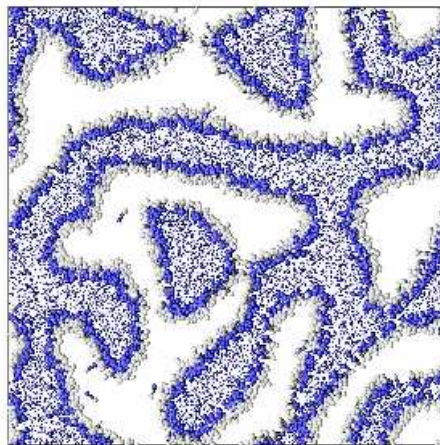


Fig. 6

Fig. 5: A snapshot showing a droplet in a mixture with  $N_A = 8,192$ ,  $N_B = 32,768$  and  $N_d = 1,500$  dimers after  $10^5$  time steps. The initial configuration is a droplet with a homogeneous distribution of dimers. The dark (blue) and light (white) colored spheres indicate the A and B particles, respectively. For clarity, A particles in the bulk are smaller, and B particles in the bulk are not shown. Parameters:  $L/a = 64$ ,  $M_A = 2$ ,  $M_B = 8$ ,  $A = 1.8$ ,  $k_B T = 0.0001$ ,  $\tau = 1$  and  $a = 1$ .

Fig. 6: Typical configuration showing the bicontinuous phase for  $N_A = N_B = 20,480$  and  $N_d = 3,000$ . Parameters:  $L/a = 64$ ,  $M_A = 5$ ,  $M_B = 5$ ,  $A = 1.8$ ,  $k_B T = 0.0001$ ,  $\tau = 1$  and  $a = 1$ .

## REFERENCES

- [1] FRISCH U., HASSLACHER B., and POMEAU Y., *Phys. Rev. Lett.*, **56** (1986) 1505.
- [2] SUCCI S., *The Lattice Boltzmann Equation for Fluid Dynamics and Beyond*. Oxford University Press, Oxford (2001).
- [3] HOOGERBRUGGE P. J. and KOELMAN J. M. V. A., *Europhys. Lett.*, **19** (1992) 155.
- [4] GROOT R. D. and WARREN P. B., *J. Chem. Phys.*, **107** (1997) 4423.
- [5] ESPANOL P. and REVENGA M., *Phys. Rev. E*, **67** (2003) 026705.
- [6] MALEVANETS A. and KAPRAL R., *J. Chem. Phys.*, **110** (1999) 8605; **112** (2000) 7260.
- [7] PADDING J. T. and LOUIS A. A., *Phys. Rev. Lett.*, **93** (2004) 220601.
- [8] FALCK E., PUNKKINEN O., VATTULAINEN I., and ALA-NISSILA T., *Phys. Rev. E*, **68** (2003) 050102(R).
- [9] MUSSAWISADE K., RIPOLL M., WINKLER R. G., and GOMPPER G., *J. Chem. Phys.*, **123** (2005) 144905.
- [10] NOGUCHI H. and GOMPPER G., *Phys. Rev. Lett.*, **93** (2004) 258102.
- [11] IHLE T., TÜZEL E., and KROLL D. M., *Phys. Rev. E*, **70** (2004) 035701(R); **72** (2005) 046707.
- [12] POOLEY C. M. and YEOMANS J. M., *J. Phys. Chem. B*, **109** (2005) 6505.
- [13] TÜZEL E., IHLE T., and KROLL D. M., *Phys. Rev. E*, **74** (2006) 056702.
- [14] IHLE T., TÜZEL E., and KROLL D. M., *Europhys. Lett.*, **73** (2006) 664.
- [15] TÜZEL E., IHLE T., and KROLL D. M., *Math. Comput. Simulat.*, **72** (2006) 232.
- [16] ROWLINSON J. S. and WIDOM B., *Molecular Theory of Capillarity*. Dover Publications, New York (2002).
- [17] IHLE T. and KROLL D. M., *Phys. Rev. E*, **63** (2001) 020201(R).
- [18] IHLE T. and TÜZEL E., *Prog. Comp. Fluid. Dyn., cond-mat/0610350*, (in press).
- [19] IHLE T. and KROLL D. M., *Phys. Rev. E*, **67** (2003) 066705.
- [20] RYDER J. F., *Mesoscopic Simulations of Complex Fluids*. PhD thesis University of Oxford (2005).
- [21] CALLEN H. B., *Thermodynamics*. Wiley, New York (1960).
- [22] TÜZEL E., *Particle-based Mesoscale Modeling of Flow and Transport in Complex Fluids*. PhD thesis University of Minnesota (2006).